J Mol Model (2013) 19:2057–2067
DOI 10.1007/s00894-012-1633-7

ORIGINAL PAPER

# Topological analysis of tetraphosphorus oxides ($P_4O_{6+n}$ (n=0–4))

**Nancy Y. Acelas · Diana López · Fanor Mondragón · William Tiznado · Elizabeth Flórez**

Received: 31 May 2012 / Accepted: 5 October 2012 / Published online: 23 October 2012


**Abstract** Quantum chemical calculations were used to analyze the chemical bonding and the reactivity of phosphorus oxides ($P_4O_{6+n}$ (n=0–4)). The chemical bonding was studied using topological analysis such as atoms in molecules (AIM), electron localization function (ELF), and the reactivity using the Fukui function. A classification of the P-O bonds formed in all structures was done according to the coordination number in each P and O atoms. It was found that there are five P-O bond types and these are distributed among the five phosphorus oxides structures. Results showed that there is good agreement among the evaluated properties (length, bond order, density at the critical point, and disynaptic population) and each P-O bond type. It was found that regardless of the structure in which a P-O bond type is present the topological and geometric properties do not have a significant variation. The topological parameters electron density and Laplacian of electron density show excellent linear correlation with the average length of P-O bond in each bond type for each structure. From the Fukui function analysis it was possible to predict that from $P_4O_6$ until $P_4O_8$ the most reactive regions are basins over the P.

**Keywords** Atoms in molecules · DFT · The Fukui function · Topological analysis

## Introduction

Knowledge of the chemistry of phosphorus oxides ($P_4O_{6+n}$ (n=0–4)) as well as the nature of chemical bonding, stability and reactivity is important in order to understand their polymerization processes [1, 2], to improve their technological applications as a basis in zeotypes, glasses, or semiconductors and the formation of ozonide from phosphorus oxides [3, 4].

Phosphorus oxides are formed during combustion reactions of elemental phosphorus or substances where phosphorus is present. $P_4O_6$ called tetraphosphorus hexoxide is formed by heating of white phosphorus in the presence of a limited amount of oxygen, and $P_4O_{10}$ which is called tetraphosphorus decaoxide is formed under the same conditions but with oxygen in excess [5]. During thermal processes, these oxides can generate stable intermediates such as $P_4O_7$, $P_4O_8$ and $P_4O_9$ [6].

These structures have been experimentally characterized by electron diffraction, X-ray diffraction, IR and Raman spectroscopy [7–9]. From X-ray studies a type cage structure for these oxides has been determinated [10]. From IR and Raman spectroscopy analysis different frequencies have been found. However, the assignation of these vibrational modes is limited. For this reason, in the last years, the characterization of these structures have been done using electronic structure methods such as density functional theory (DFT) [7, 11, 12]. For example, Carbonniere and Pouchan [5], used a DFT anharmonic approach to obtain the vibrational spectrum of $P_4O_6$ and $P_4O_{10}$. Valentim et al. [10], studied the vibrational spectrum of ($P_4O_{6+n}$ (n=0–4)) to characterize changes in the binding properties in these series of oxides. Mowrey et al. [11] used ab-initio methods

**Electronic supplementary material** The online version of this article (doi:10.1007/s00894-012-1633-7) contains supplementary material, which is available to authorized users.

N. Y. Acelas · D. López · F. Mondragón (✉)
Institute of Chemistry, University of Antioquia,
A.A. 1226, Medellín, Colombia
e-mail: fmondra@gmail.com

W. Tiznado
Departamento de Ciencias Químicas, Facultad de Ciencias,
Universidad Andres Bello,
Av. República 275,
Santiago, Chile

E. Flórez
Department of Basic Sciences, University of Medellin,
A.A 1226, Medellín, Colombia

to calculate optimized molecular geometries and the vibrational frequencies for the interpretation of the infrared spectra for $P_4O_6$ and $P_4O_{10}$.

To the knowledge of the authors, a detailed analysis of the chemical bonding as well as the reactivity of each one of these structures have not been discussed in the scientific literature. In this study, we characterized theoretically the phosphorus oxides ($P_4O_{6+n}$ (n=0–4)), using electronic structure methods. A topological analysis (atoms in molecules (AIM), electron localization function (ELF), and Fukui function) was focused on the different bonds type (P-O) in all phosphorus oxides structures.

## Computational details

To determine the theoretical model and basis set, the phosphorous oxide (PO) molecule was chosen for the preliminary calculations, and the results were compared with experimental and computational data reported in the literature [13]. Bond lengths, frequencies, dipole moments, ionization potential and electron affinity were determined using different theoretical models and basis sets. Table 1 shows the data calculated at different theoretical models and basis sets for the PO molecule. In all cases the results obtained with the basis aug-cc-pcvtz are the closest to the experimental values. Comparing the results using B3LYP/aug-cc-pcvtz with the experimental results the differences are 0.2 %, 1.9 %, 3.6 %, and 5.5 % for bond distance, vibrational frequency, ionization potential and electron affinity, respectively. Also, comparing these results with a more correlated theoretical model and a larger basis set (CCSD (T) / aug-cc-pvqz), it is observed that the variations of the above properties are between 0.4 % and 4.4 %. This suggests that the model B3LYP/aug-cc-pcvtz can satisfactorily describe the electronic properties of phosphorus oxides without a high computational cost.

Considering that there are not significant changes, the data shown in this work were calculated using the B3LYP model and the aug-cc-pcvdz basis set. All the calculations were carried out using the Gaussian 03 software package.

## Topological analysis

In order to analyze the chemical bonding and reactivity of the systems investigated; we used of the electron localization functions (ELF), atoms in molecules theory (AIM), and the condensed Fukui function $\left(f_{Ff}^{-/+}\right)$.

**Table 1** Optimized distances ($r_e$), frequencies ($\omega$), dipole moment, ($\mu$), ionization potential (IP), and electron affinity (EA)

| Theory level/basis sets | re (Å) | ω ($cm^{-1}$) | μ (debye) | IP (eV) | EA (eV) |
|---|---|---|---|---|---|
| HF | | | | | |
| 6–311g(d,p) | 1.448 | 1416.41 | 2.72 | 8.14 | 0.310 |
| 6–311++g(d,p) | 1.449 | 1407.96 | 2.79 | 8.27 | 0.660 |
| cc-aug-pcvdz | 1.471 | 1356.23 | 2.50 | 8.40 | 0.730 |
| cc-aug-pcvtz | 1.441 | 1435.76 | 2.38 | 8.29 | 0.608 |
| B3LYP | | | | | |
| 6–311g(d,p) | 1.492 | 1235.45 | 2.20 | 8.57 | 0.764 |
| 6–311++g(d,p) | 1.492 | 1232.67 | 2.33 | 8.71 | 1.165 |
| cc-aug-pcvdz | 1.512 | 1194.07 | 2.08 | 8.78 | 1.228 |
| cc-aug-pcvtz | 1.480 | 1256.45 | 2.03 | 8.69 | 1.152 |
| PW91PW91 | | | | | |
| 6–311g(d,p) | 1.507 | 1055.19 | 1.98 | 7.36 | 2.216 |
| 6–311++g(d,p) | 1.508 | 1054.22 | 2.12 | 7.51 | 2.518 |
| cc-aug-pcvdz | 1.528 | 1093.63 | 1.89 | 8.66 | 1.213 |
| cc-aug-pcvtz | 1.495 | 1207.57 | 1.84 | 8.71 | 1.240 |
| MP2 | | | | | |
| 6–311g(d,p) | 1.468 | 3761.59 | 2.81 | 7.57 | 0.036 |
| 6–311++g(d,p) | 1.473 | 3185.92 | 2.91 | 7.75 | 0.519 |
| cc-aug-pcvdz | 1.543 | 1355.42 | 2.88 | 8.11 | 0.911 |
| cc-aug-pcvtz | 1.493 | 1298.66 | 2.66 | 8.18 | 0.930 |
| CCSD(T)[f] cc-aug-pvqz | 1.487 | 1229.00 | 2.63 | 8.36 | 1.103 |
| Exp | 1.476[a] | 1233.37[b] | 1.88±0.07[c] | 8.39±001[d] | 1.092[e] |

[a,b] Reference [14], [c] Reference [15], [d] Reference [16], [e] Reference [17], [f] Reference [13]

### Electron localization function

The value of ELF at any point in space is calculated from the kinetic energy associated with ρ(r) at that point and is scaled to range from 0 to 1. Regions where the ELF has higher values (> 0.5) tend to be associated with electron pairs, such as bonds, lone pair, and core electrons. For the purpose of the current study, it is useful to examine isosurfaces in the ELF distribution corresponding to such higher ELF values and to identify the locations of the regions or "basins" (a basin is the volume of space enclosed by an isosurface of specified value) that can be related to "electron pairs," and hence to bonds. The electron population in each basin can be integrated, and the resulting value is related to the chemical understanding of any bond associated. The (ELF) of Becke and Edgecombe were calculated using the TopMod [18] programs set and visualized with the MOLEKEL 5.3 program [19].

### Atoms in molecules (AIM) analysis

The topological analysis was proposed by Bader in his theory, quantum theory of atoms in molecules [20]. It permits us to analyze the nature of the bond formed in the molecule or complex. This can be implemented through the study of electron density-based topological parameters, such as the values of the electron density and its Laplacian at the bond critical points (BCP).

A BCP (point corresponding to $\nabla\rho(r)=0$) is found between each pair of nuclei, which is considered to be linked by a chemical bond. The bond ellipticity defined in terms of the two negative curvatures as $\varepsilon=(\lambda_1/\lambda_{2-1})$ reflects the deviation of the charge distribution of a bond path from axial symmetry, thus providing a sensitive measure of the susceptibility of a system undergoing structural changes.

The Laplacian of the electron density ($\nabla^2\rho(r)$) indicates if the electron density is locally concentrated ($\nabla^2\rho<0$) or depleted ($\nabla^2\rho>0$). A negative value of $\nabla^2\rho(r)$ at the BCP or high values of ρ(r) are associated to the covalent character of bond, indicating sharing of electrons and is known as shared interactions. A positive value of $\nabla^2\rho(r)$ at the BCP or low ρ(r) values (< 0.1 atomic units), implies closed-shell type interactions found in ionic bonds, hydrogen bonds, and van der Waals molecules. Molecular graphs (sets of bond paths, BPs, which are lines of maximum ρ linking the nuclei arrangement in stable structures) of phosphorus oxides ($P_4O_{6+n}$ (n=0–4)) were obtained using the MORPHY 98 program [21].

Wave functions (as the only input information required for the topological analysis) were calculated with the same approach used for the optimization and frequency calculations. The topological properties evaluated were: electron density ρ(r), Laplacian $\nabla^2\rho(r)$ and bond ellipticity (ε) at bond critical point (BCP) of the bond paths representing the formation of each type of P-O bonds in phosphorus oxides.

### Fukui function

In the density-functional theory approach to phenomenological chemical reactivity theory (chemical DFT) [22–25], the reactive site of an acceptor of electrons is associated with a large positive value of the Fukui function [26, 27].

$$f^{+}(r)=\left(\frac{\partial\rho(r)}{\partial N}\right)^{+}_{v(r)}=\rho_{N+1}(r)-\rho_N(r) \quad (1)$$

The superscript "+" on the derivative indicates that the derivative is taken from above; this is essential because the derivative from above and the derivative from below,

$$f^{-}(r)=\left(\frac{\partial\rho(r)}{\partial N}\right)^{-}_{v(r)}=\rho_N(r)-\rho_N(r) \quad (2)$$

are not equal when the number of electrons is an integer, owing to the derivative discontinuity of the energy [28, 29], density, and other molecular properties [30, 31]. Similarly, the Fukui function from below is the key regioselectivity indicator for donor of electrons.

The link between the chemical DFT description and the frontier MO theory description is clear when one approximates the Fukui functions using the frontier molecular orbitals [32, 33],

$$f^{-}(r)=|\emptyset_{HOMO}(r)|^2 \quad f^{+}(r)=|\emptyset_{LUMO}(r)|^2 \quad (3)$$

These approximations are sufficient except for the seemingly rare cases where orbital relaxation effects are important [34–36]. When the highest occupied molecular orbital (HOMO) or lowest unoccupied molecular orbital (LUMO) belongs to a degenerate irreducible representation of the cluster´s point goup an average over the set of degenerated orbitals is used [37–39].

Associated to the Fukui function there is a gradient vector field, $\nabla f(r)$. This field is characterized by so-called critical points, where $\nabla f(r)=(0,0,0)$. They represent local maxima, minima and saddle points of $f(r)$. From a Hessian matrix, H($f(r_c)$), analysis associated to each critical point define four different types of nondegenerate critical points: attractor (3, −3), repellor (3, 3), and saddle points (3, 1) and (3, −1). A basin, roughly speaking is a region of the space, Ω, given by all points whose gradient paths end at the same attractor. The integral of the Fukui function in each basin, $f_k$, is a measure of the "abundance (population)" of the Fukui function around the attractor $k$. The topological analysis of the Fukui function was been recently proposed [40–42] and

probed and has proven to be a useful tool to describe reactivity of classic [43–45] and exotic chemical systems.

The $f_{Ff}^{-/+}$ condensed Fukui function has been evaluated using DGrid 4.4 set of programs [46].

## Results and discussion

### Geometric parameters

The geometric parameters of diphosphorus oxides were evaluated to have a first approach to tetraphosphorus oxides. Diphosphorus oxides studied were $P_2O$, $P_2O_2$, $P_2O_3$, $P_2O_4$, $P_2O_5$ [12]. Singlet and triplet multiplicities were evaluated. The results concerning the isomers and relative energies, with reference to the most stable structure of diphosphorus oxides can be found in Table S1 in the Supplementary material.

The geometric parameters of diphosphorus oxides are discussed in order of increasing the number of oxygen atoms from $P_2O$ to $P_2O_5$ (see Table S2 in Supplementary material where the geometric parameters from more stable diphosphorus oxides can be found). The $P_2O$ and $P_2O_2$ structures have one and two dimensions, respectively. From $P_2O_3$ to $P_2O_5$ three dimension structures are more favorable, and the formation of the P-O-P oxo-bridged bond is favorable instead of P-P bond formation. With the increasing of oxygen atoms in each structure the P-P bond begins to weaken, this observation is in agreement with the P-P bond lengths, from 1.89 Å for $P_2O$ and 2.12 Å from $P_2O_5$.

The initial structures of phosphorus oxides ($P_4O_{6+n}$ (n=0–4)) were taken from experimental data reported in the literature [6, 7]. Harmonic vibrational frequencies of these structures were calculated at the same level of theory and were subsequently performed on the geometry optimized structures corresponding to stationary points on the potential energy surface to verify that an energy minimum has been achieved (i.e., no imaginary frequencies).

Figure 1 and Table 2 show the optimized structures and the geometric parameters of tetraphosphorus oxides, respectively. The results show that the computational results are in good agreement with the experimental available data. It can be observed that according to the coordination number of phosphorus and oxygen atoms different kinds of P-O bonds can be found. $P_4O_7$ and $P_4O_8$ structures are those with greater P-O bonds variability. The bond length for each type of bond is independent of the oxygen atoms number in the structure, for example, $P^{III}$-$O_c$ length is around 1.47 Å for all of these structures: $P_4O_8$, $P_4O_9$ and $P_4O_{10}$. It is noteworthy that the geometric model found in $P_4O_6$ (Fig. 1), is the structural basis for the formation of other tetra-phosphorus oxides, having as the main unit the $P_4$ tetrahedron and the oxygen atoms serving as a bridge to join each phosphorus atom. This model is in accordance with the results found by Engels et al. [2], where for oxygen-rich compounds $P_4O_n$ (n=4–6) the stability of the P-O-P unit in comparison to the stability of one P-P single and one terminal P=O double bond, determines the structures of the energetically most favorable isomers. Similarly, as the number of oxygen atoms increases the number of phosphorus atoms with coordination number of 3 decreases and the

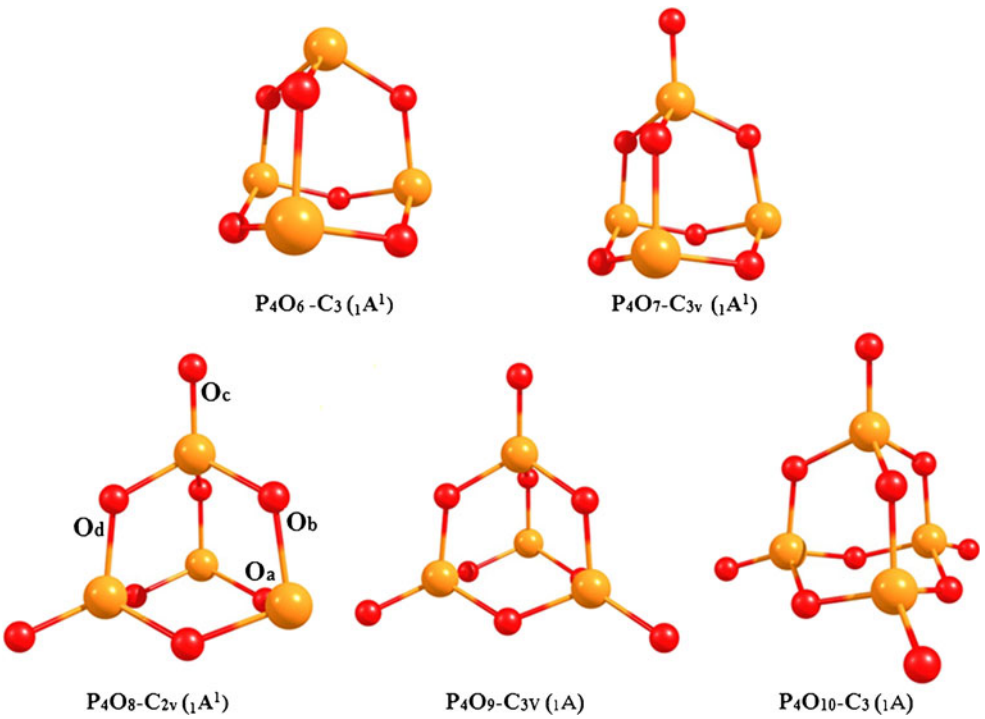


**Fig. 1** Structures optimized with B3LYP theory level and aug-ccpvdz basis set for $P_4O_6$, $P_4O_7$, $P_4O_8$, $P_4O_9$ and $P_4O_{10}$. $O_a$, $O_b$ and $O_d$ are bridging oxygen between $P^{III}/P^{III}$, $P^{III}/P^{V}$ and $P^{V}/P^{V}$, respectively; $O_c$ is in a terminal position

**Table 2** Geometric parameters of tetraphosphorus oxides calculated with B3LYP/ aug-cc-pcvdz

| Structure | Bond lengths (pm) | Bond angle | Experimental data |
|---|---|---|---|
| $P_4O_6$ | $P^{III}$-$O_a$: 169.8 | $P^{III}$-$O_a$-$P^{III}$: 126 | $P^{III}$-$O_a$: 163.8 |
| | | $O_a$-$P^{III}$-$O_a$ : 100 | $P^{III}$-$O_a$-$P^{III}$: 126.7 |
| | | | $O_a$-$P^{III}$-$O_a$ : 99.8 |
| $P_4O_7$ | $P^{III}$ – $O_a$: 169.5 | $P^{III}$-$O_a$-$P^{III}$: 126 | $P^{III}$ – $O_a$: 164.4 |
| | $P^{III}$ – $O_b$: 171.1 | $O_a$-$P^{III}$-$O_a$ : 100 | $P^{III}$ – $O_b$: 168.4 |
| | $P^{V}$ – $O_b$: 164.5 | $P^{III}$-$O_b$-$P^{V}$: 124 | $P^{V}$ – $O_b$: 159.5 |
| | $P^{V}$ – $O_c$: 147.9 | $O_b$-$P^{V}$-$O_c$: 115 | $P^{V}$ – $O_c$: 145.0 |
| $P_4O_8$ | $P^{III}$ – $O_a$: 169.2 | $P^{III}$-$O_a$-$P^{III}$: 127 | $P^{III}$ – $O_a$: 163.3 |
| | $P^{III}$ – $O_b$: 170.8 | $P^{III}$-$O_b$-$P^{V}$: 124 | $P^{III}$ – $O_b$: 166.8 |
| | $P^{V}$ – $O_b$: 164.5 | $O_b$-$P^{V}$-$O_c$: 116 | $P^{V}$ – $O_b$: 157.6 |
| | $P^{V}$ – $O_c$: 147.6 | $O_b$-$P^{III}$-$O_b$: 99 | $P^{V}$ – $O_c$: 141.4 |
| | $P^{V}$ – $O_d$: 165.5 | $P^{V}$-$O_d$-$P^{V}$: 123 | |
| | | $O_b$-$P^{V}$-$O_d$: 102 | |
| $P_4O_9$ | $P^{III}$ – $O_b$: 170.5 | $P^{III}$-$O_b$-$P^{V}$: 124 | $P^{III}$ – $O_b$: 166.1 |
| | $P^{V}$ – $O_b$: 164.5 | $O_b$-$P^{V}$-$O_c$: 117 | $P^{V}$ – $O_b$: 160.5 |
| | $P^{V}$ – $O_c$: 147.3 | $O_b$-$P^{III}$-$O_b$: 100 | $P^{V}$ – $O_c$: 141.8 |
| | $P^{V}$ – $O_d$: 165.5 | $P^{V}$-$O_d$-$P^{V}$: 123 | |
| | | $O_b$-$P^{V}$-$O_d$: 102 | |
| $P_4O_{10}$ | $P^{V}$ – $O_c$: 147.2 | $O_b$-$P^{V}$-$O_c$: 116 | $P^{V}$ – $O_c$: 142.9 |
| | $P^{V}$ – $O_d$: 165.4 | $P^{V}$-$O_d$-$P^{V}$: 123 | $P^{V}$ – $O_d$: 160.4 |
| | | | $O_b$-$P^{V}$-$O_c$: 116.5 |
| | | | $P^{V}$-$O_d$-$P^{V}$: 123.5 |

$P^{III}$ and $P^{V}$ correspond to phosphorus atoms in 3 and 5 coordination number, respectively.

$O_a$ , $O_b$ and $O_d$ are bridging oxygen between $P^{III}/P^{III}$ , $P^{III}/P^{V}$ and $P^{V}/P^{V}$, respectively;

$O_c$ is in a terminal position.

Experimental data [7]: $P_4O_7$, $P_4O_8$ and $P_4O_9$

Experimental data [5]: $P_4O_6$ and $P_4O_{10}$

coordination number of 5 increases, therefore the $P_4O_6$ has no phosphorus atoms with coordination number of 5 and the $P_4O_{10}$ has no phosphorus atoms with coordination number of 3.

## Electronic properties

The calculated electronic properties were: ionization potential and HOMO-LUMO gap.

The ionization potential was calculated by the finite differences between the energy of the neutral and cationic specie (cation in the geometry of the neutral structure) and the Koopman approximation.

$$IP_{(P_nO_m)} = E_{(P_nO_m{}^{+})} - E_{(P_nO_m)}$$

$$IP_{(P_nO_m)} - E_{HOMO(P_nO_m)}$$

The HOMO-LUMO gap for tetraphosphorus and diphosphorus oxides was calculated using the frontier orbitals energies:

$$GAP = E_{HOMO(P_nO_m)} - E_{LUMO(P_nO_m)}$$

where $E_{HOMO}$ indicates the highest occupied molecular orbital energy and $E_{LUMO}$ the lowest unoccupied molecular orbital energy.

Figure 2 and S1 in the Supplementary material show the ionization potential and the HOMO-LUMO gap for tetraphosphorus and diphosphorus oxides, respectively. It can be seen that by increasing the number of oxygen atoms, the ionization potential and HOMO-LUMO gap also increase for both diphosphorus and tetraphosphorus oxides. In the case of diphosphorus there is an exception with $P_2O_2$ structure in which both the ionization potential and HOMO-LUMO gap decreases. This could be due to the fact that it presents triplet multiplicity. Therefore, there are unpaired electrons and hence the structure requires less energy to donate them with respect to a closed shell where there are paired spins and the ionization potential is greater.

The order from low to high ionization potential for the tetraphosphorus oxides is: $P_4O_6<P_4O_7<P_4O_8<P_4O_9<P_4O_{10}$. This order could be explained by the fact that the addition of an electronegative element in the compound more strongly bind the electrons and thus make it more difficult to ionize. The same trend is observed in the increase in the HOMO-LUMO gap when moving from $P_4O_8$ to $P_4O_9$. Large gaps are indicative of stability, and then this indicates that the $P_4O_9$ and $P_4O_{10}$ are much more resistant to the transfer of electrons than smaller systems.

## Bonding and local reactivity analysis

### *Natural bonding orbital (NBO)*

Table 3 presents the charges and bond orders calculated by population analysis (NBO) and electronic configuration for tetraphosphorus oxides.

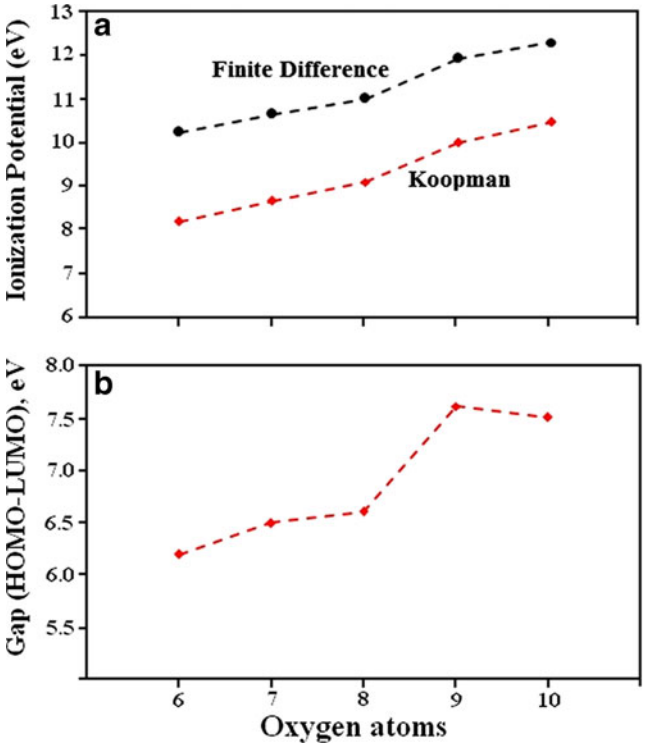


**Fig. 2** **a**) Ionization potential for tetraphosphorus oxides and **b**) HOMO-LUMO gap (HOMO-LUMO)

As expected, independent of the structure there was not variation in the bond order for each type of bond, which agrees with the observation at the geometric parameters. The bond orders between $P^{III}$-$O_a$, $P^{III}$-$O_b$, $P^V$-$O_b$ and $P^V$-$O_d$ vary from 0.64 to 0.69 which indicates an approach to single bonds. The $P^V$-$O_c$ bond type, present from $P_4O_7$ to $P_4O_{10}$ structures, has a bond order value that varies from 1.36 to 1.43 which corresponds approximately to a double bond, which suggests a stronger bond. Regarding the charges, it can be seen that the negative charges are on the oxygen atoms and the charge on the phosphorus III atoms is less than the charge on the phosphorus V atoms, which is due to the presence of more oxygen atoms.

From an overview of the electronic configuration, for all tetraphosphorus oxides structures could be said that there is a decreasing at the electronic population of p orbitals of phosphorus atoms and there is an increasing at the electronic population of p orbitals of the oxygen atoms. It could suggest that bond formation takes place by electron density displacement from the phosphorus atom to the oxygen atom. That displacement is related to the bond type of phosphorus atoms in each structure, where phosphorus atoms with coordination number of 5 have more electron density displacement than phosphorus atoms with coordination number of 3. This could be explained by the donation of two electrons

**Table 3** Bond orders and charges for tetraphosphorus oxides, calculated with B3LYP/aug-cc-pcvdz

| Structure | Electronic configuration | | |
|---|---|---|---|
| | P: 3 $s^2$ $3p^3$<br>O: 2 $s^2$ $2p^4$ | Bond order | Charges NBO |
| $P_4O_6$ | $P^{III}$: 3 s(1.55)3p(1.72) | $P^{III}$-$O_a$: 0.6781 | $P^{III}$: 1.67007 |
| | $O_a$: 2 s(1.78)2p(5.29) | | $O_a$: -1.11354 |
| $P_4O_7$ | $P^V$: 3 s(0.76)3p(1.55) | $P^{III}$ – $O_a$: 0.6824 | $P^{III}$: 1.68358 |
| | $P^{III}$: 3 s(1.57)3p(1.70) | $P^{III}$ – $O_b$: 0.6477 | $P^V$: 2.60523 |
| | $O_a$: 2 s(1.78)2p(5.29) | $P^V$ – $O_b$: 0.6618 | $O_a$: -1.10993 |
| | $O_b$: 2 s(1.77)2p( 5.28) | $P^V$ – $O_c$: 1.3649 | $O_b$: -1.10422 |
| | $O_c$: 2 s(1.82)2p( 5.14) | | $O_c$: -1.01352 |
| $P_4O_8$ | $P^V$: 3 s(0.77)3p(1.55) | $P^{III}$ – $O_a$: 0.6869 | $P^{III}$: 1.69745 |
| | $P^{III}$: 3 s (1.58)3p(1.68) | $P^{III}$ – $O_b$: 0.6535 | $P^V$: 2.59993 |
| | $O_a$: 2 s(1.78)2p(5.29) | $P^V$ – $O_b$: 0.6637 | $O_a$: -1.10555 |
| | $O_b$: 2 s(1.77)2p(5.28) | $P^V$ – $O_c$: 1.3867 | $O_b$: -1.09916 |
| | $O_c$: 2 s(1.82)2p(5.13) | $P^V$ – $O_d$:0.6334 | $O_c$: -1.00068 |
| | | | $O_d$: -1.09120 |
| $P_4O_9$ | $P^V$: 3 s(0.77)3p(1.56) | $P^{III}$ – $O_b$: 0.6595 | $P^{III}$: 1.71201 |
| | $P^{III}$: 3 s(1.58)3p(1.66) | $P^V$ – $O_b$: 0.6652 | $P^V$: 2.59419 |
| | $O_b$: 2 s(1.77)2p(5.27) | $P^V$ – $O_c$: 1.4090 | $O_b$: -1.09321 |
| | $O_c$: 2 s(1.82)2p(5.11) | $P^V$ – $O_d$: 0.6369 | $O_c$: -0.98621 |
| | | | $O_d$: -1.08545 |
| $P_4O_{10}$ | $P^V$: 3 s(0.77)3p(1.56) | $P^V$ – $O_c$: 1.4296 | $P^V$: 2.59054 |
| | $O_c$: 2 s(1.82)2p(5.10) | $P^V$ – $O_d$: 0.6406 | $O_c$: -0.97241 |
| | $O_d$: 2 s(1.77)2p(5.26) | | $O_d$: -1.07878 |

$P^{III}$ and $P^V$ correspond to phosphorus atoms in 3 and 5 coordination numbers, respectively

$O_a$ , $O_b$ and $O_d$ are bridging oxygen between $P^{III}/P^{III}$ , $P^{III}/P^V$ and $P^V/P^V$, respectively; $O_c$ is in a terminal position

from the phosphorus V atom to the oxygen ($O_c$), where three available phosphorus electrons are used for the formation of the oxo-bridged bond ($O_a$, $O_b$ and $O_d$) and two electrons are donated to the oxygen for the formation of the $P^V$-$O_c$ terminal bond. In agreement with this observation, there is no expansion of the valence shell of the phosphorus V atom to form five bonds. The charge displacement agrees with the NBO analysis where the electron density is on the oxygen atoms.

*Atoms in molecules analysis (AIM)*

The calculated values of electron density (ρ), Laplacian of electron density ($\nabla^2\rho$), and ellipticity (ε) at BCP of each bond type in tetraphosphorus molecules are presented in Table 4. The complete set of molecular graphs for the tetraphosphorus oxides are shown in Fig. 3. $P_4O_7$ molecule in Fig. 3 is used to display an example of ring critical point (RCP), bond critical point (BCP) and bond path (BP) as expected topological characteristics besides the nuclear positions according to the adopted geometry for that structure.

In the present study the value of ρ and $\nabla^2\rho$ varies from 0.1342–0.2278 to 0.4110–1.6013 a.u, respectively. It can be seen that there are no variations for these properties in each type of bond for the different tetraphosphorus oxides structures, and these results are in agreement with the results shown in previous sessions. Comparing the electron density (ρ) at the BCP from one type of bond to another in tetraphosphorus oxides, it could be related to bond order. $P^{III}$-$O_a$, $P^{III}$-$O_b$, $P^V$-$O_b$, $P^V$-$O_d$ bonds provide prototypes of a single bond (ρ ~0.15 a.u) while $P^V$-$O_c$ bond has character of a double bond (ρ ~0.22 a.u). It can be seen ρ increases for the last ones and that $\nabla^2\rho$ becomes increasingly more positive. These two factors lead to the conclusion that the extent of charge accumulation between the nuclei increases with the bond order, or assumed number of electron pair bonds [47]. It is expected that strong bonds like $P^V$-$O_c$ (1.47 Å) are usually associated with high electron density values indicating higher structural stability. This could give us an idea that the structure of tetraphosphorus oxide which is more stable is $P_4O_{10}$ which has a larger quantity of $P^V$-$O_c$ bonds.

Furthermore, we have been able to establish a correlation between the P-O bond distances in each type, electron density (ρ) and Laplacian of electron density ($\nabla^2\rho$). The curves corresponding to the correlation fit are shown in Fig. 4. The correlation between bond length and electron density is inverse, that is, an increase in bond length corresponds to a decrease in the electron density, which is expected, since an increase in distance results in reduced orbital overlap and hence, low electron density along the bond. The P-O bond length and the Laplacian correlation is also inverse and analogous to electron density. The correlation coefficient value for the electron density and its Laplacian with P-O bond distance are: 0.994 and 0.995, respectively.

*Electron localization function (ELF)*

Figure 5 presents the domains with high ELF values and the presence of lone pairs monosynaptic valence basins located at each O atom.

Table 5 shows the monosynaptic and disynaptic population analysis for tetraphosphorus oxides. For monosynaptic basins the electronic population varies from 5.93 to 6.27 for $P_4O_7$ and $P_4O_{10}$, respectively, in the type c oxygen ($O_c$).

**Table 4** Topological analysis of electron density (*ρ*), laplacian of electron density ($\nabla^2\rho$), and ellipticity (ε) calculated using B3LYP/aug-cc-pcvdz

| Molecule | Type of bond | R(Å) | ρ(r) | $\nabla^2\rho(r)$ | ε |
|---|---|---|---|---|---|
| $P_4O_6$ | $P^{III}$-$O_a$ | 1.698 | 0.13849 | 0.45137 | 0.09235 |
| $P_4O_7$ | $P^{III}$-$O_a$ | 1.695 | 0.13901 | 0.46051 | 0.08793 |
| | $P^{III}$-$O_b$ | 1.711 | 0.13420 | 0.41101 | 0.08730 |
| | $P^V$-$O_b$ | 1.645 | 0.15442 | 0.65898 | 0.01787 |
| | $P^V$-$O_c$ | 1.479 | 0.22409 | 1.56289 | 0.00002 |
| $P_4O_8$ | $P^{III}$-$O_a$ | 1.697 | 0.13801 | 0.45541 | 0.08443 |
| | $P^{III}$-$O_b$ | 1.708 | 0.13497 | 0.42201 | 0.08974 |
| | $P^V$-$O_b$ | 1.645 | 0.15462 | 0.65890 | 0.02075 |
| | $P^V$-$O_c$ | 1.476 | 0.22552 | 1.58072 | 0.00305 |
| | $P^V$-$O_d$ | 1.657 | 0.14980 | 0.61324 | 0.02465 |
| $P_4O_9$ | $P^{III}$-$O_b$ | 1.705 | 0.13572 | 0.43123 | 0.09012 |
| | $P^V$-$O_b$ | 1.645 | 0.15465 | 0.65439 | 0.02245 |
| | $P^V$-$O_c$ | 1.473 | 0.22682 | 1.59561 | 0.00180 |
| | $P^V$-$O_d$ | 1.655 | 0.15023 | 0.62031 | 0.02218 |
| $P_4O_{10}$ | $P^V$-$O_c$ | 1.472 | 0.22780 | 1.60126 | 0.00010 |
| | $P^V$-$O_d$ | 1.654 | 0.15061 | 0.62774 | 0.01867 |

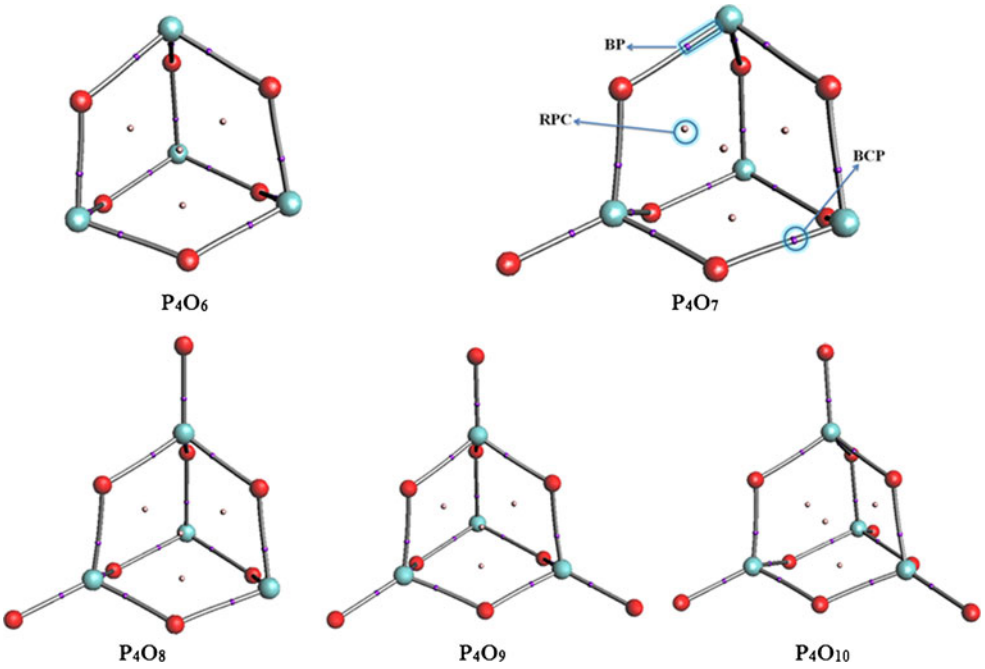


**Fig. 3** Molecular graphs of tetraphosphorus oxides. Topological terminology: RCP: ring critical point. BCP: bond critical point. BP: bond path

This increase could be due to the increase of phosphorus V atoms, with increasing the number of oxygen atoms in the structures.

From the data obtained by ELF, it can be said that the bond from these systems is covalent, as evidenced by the formation of disynaptic basins between the P-O bonds. Table 5 shows that the electronic population values for the disynaptic basins for the bonds $P^{III}$-$O_a$ and $P^{III}$-$O_b$ are in the range of 1.29–1.44 and for the bonds $P^{V}$-$O_b$, $P^{V}$-$O_c$ and $P^{V}$-$O_d$ the values vary from 1.45 to 2.06 electrons, the values for bonds with phosphorus III are lower due to the reduced availability of electrons of this atom. Similarly, it can be observed that the terminal bonds of tetraphosphorus oxides have greater strength than the bonds of the bridge type. This is in agreement with the results obtained from NBO.

The values obtained by the ELF analysis for different P-O bonds provide an indication of the reactivity of each phosphorus oxide. Higher values in disynaptic basins indicate stronger bonds between two atoms, in this case phosphorus and oxygen. As the electronic population value for the disynaptic basin decrease the P-O bond starts to become weaker. Therefore, P-O bonds with smaller values for the disynaptic basin have higher reactivity that those with higher values for the disynaptic basin.

With the reported values in Table 5 for the disynaptic basins it is possible to infer that the breaking of the bridge type bonds ($P^{III}$-$O_a$, $P^{III}$-$O_b$, $P^{V}$-$O_b$ and $P^{V}$-$O_d$) is more feasible than the breaking in the terminal bond ($P^{V}$-$O_c$). Moreover, the structures diminish their reactivity as they increase the number of oxygen atoms. This

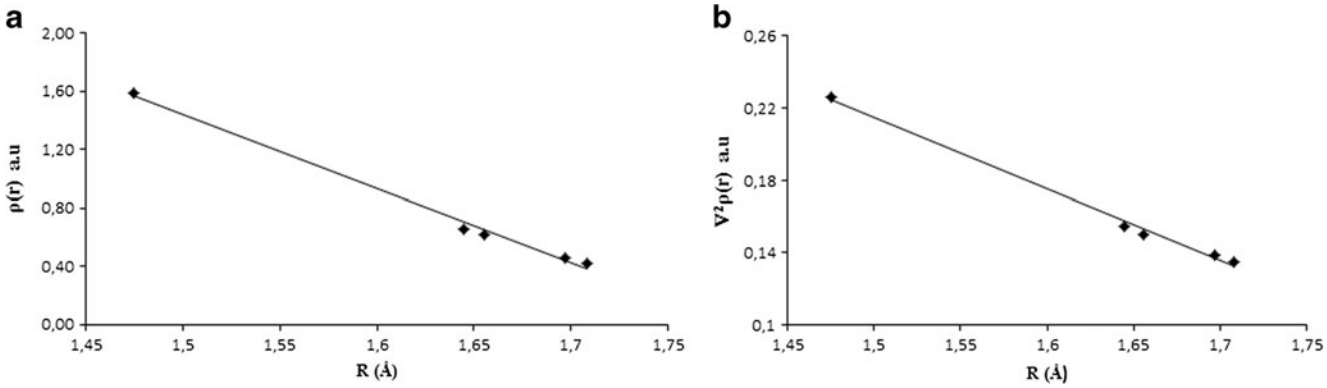


**Fig. 4** (**a**) The correlation between electron density ($\rho$(r)) at bond critical point and the average length of P-O bond in each bond type for each structure. (**b**) The correlation between the Laplacian of the density ($\nabla^2\rho$(r)) at bond critical point and the average length of P-O bond in each bond type for each structure

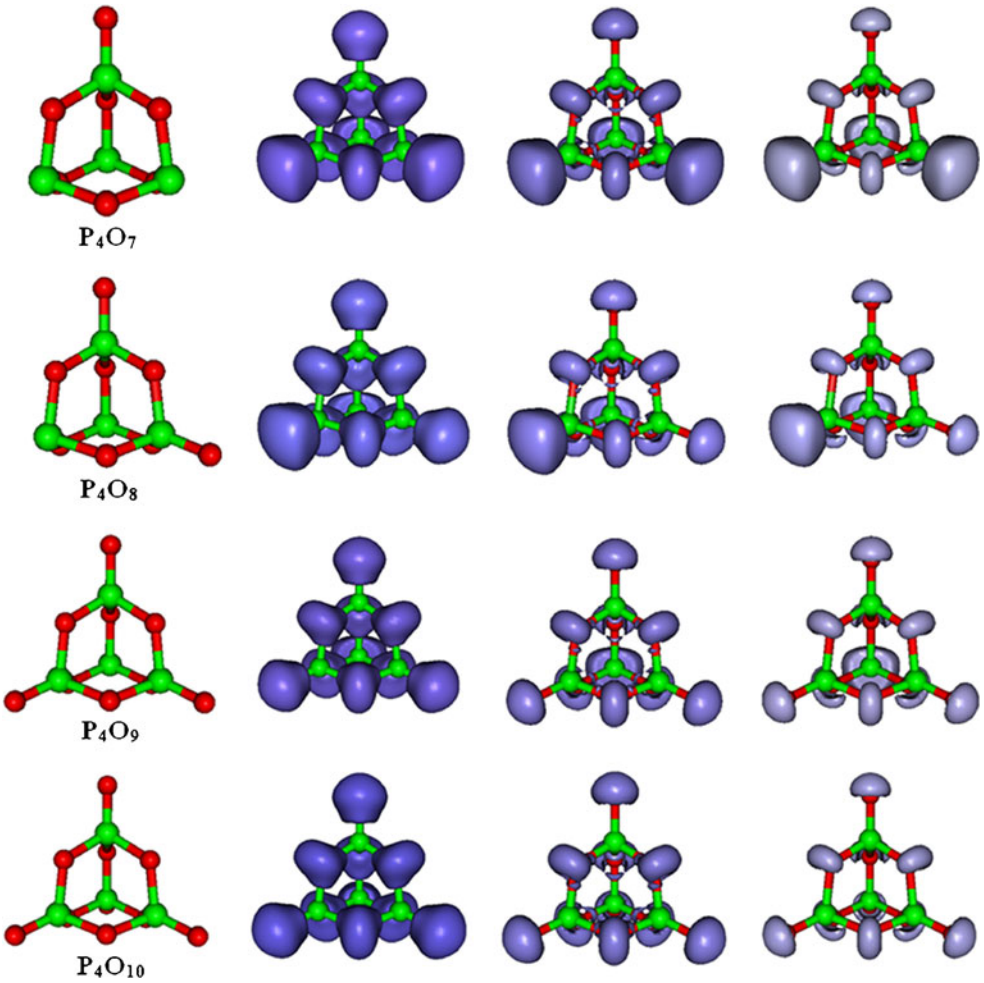


**Fig. 5** Representation of ELF localization domains. The isosurface values are 0.75, 0.82, and 0.85

can be explained by the stronger strength acquired by bridge type bond when forming the bond with phosphorus atoms in coordination number 5 which have more electrons available for bond formation.

**Table 5** Population analysis by the electron localization functions (ELF), for tetraphosphorus oxides

| Population basin | $P_4O_6$ | $P_4O_7$ | $P_4O_8$ | $P_4O_9$ | $P_4O_{10}$ |
|---|---|---|---|---|---|
| Monosynaptic | | | | | |
| ($O_a$) | 5.03 | 5.10 | 4.94 | | |
| ($O_b$) | | 4.93 | 4.99 | 4.98 | |
| ($O_c$) | | 5.93 | 5.95 | 5.93 | 6.27 |
| ($O_d$) | | | 4.99 | 4.99 | 4.93 |
| ($P^{III}$) | 2.30 | 2.30 | 2.29 | 2.30 | |
| Disypnaptic | | | | | |
| ($P^{III}$-$O_a$) | 1.33 | 1.40 | 1.44 | | |
| ($P^{III}$-$O_b$) | | 1.29 | 1.34 | 1.34 | |
| ($P^{V}$-$O_b$) | | 1.52 | 1.58 | 1.56 | |
| ($P^{V}$-$O_c$) | | 2.06 | 2.06 | 2.04 | 2.02 |
| ($P^{V}$-$O_d$) | | | 1.48 | 1.45 | 1.49 |

*Condensed Fukui function*

The results from the topological analysis of the Fukui function are show in Fig. 6. As previously described in the methodological section, this methodology allows the determination of molecular regions with chemical meaning. These regions are represented by adequate isosurfaces (in Fig. 6) with the corresponding Fukui condensed values. The interpretation is that regions (Fukui basins) with highest condensed values should be the most reactive regions susceptible (in this case) to electrophilic attack.

For the P pure cluster ($P_4$) considered in this study, the topological analysis provides 12 equivalent basins, distributed in pairs over the bonding P-P region. Therefore, the Fukui function predicts that this cluster should be more reactive in the bonding regions. For $P_4O_6$, the situation changes, four equivalent basins with characteristics of lone pairs located over each P atom are observed. Additionally 12 equivalent basins distributed in pairs over each O atom are shown. However, these regions are less reactive in terms of their small values

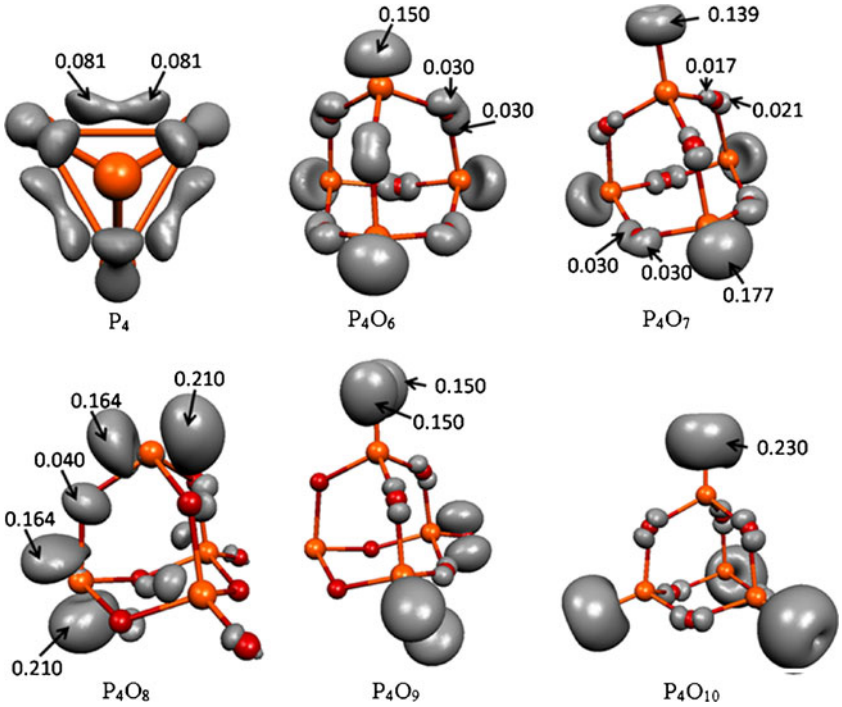


**Fig. 6** Donor Fukui functions ($f^-$) with their corresponding condensed values for $P_4O_n$ (n= 0, 6–10) global minimum structures of singlet and triplet configurations

(0.030) compared with the condensed values over the P basins (0.150).

The following cluster, $P_4O_7$, can be seen as the result of adding an oxygen atom over one of the P atoms in $P_4O_6$, this structural relationship is also manifested in the Fukui function topology, where one of the lone pair-like basins is replaced by a basin centered over the O atom, specifically, the O which is added on the region of the P lone pair. It is important to remark, that the most reactive regions are basins over the P, this reactivity behavior continues in $P_4O_8$, the Fukui function describes the P atoms as the most reactive regions on the cluster, but there are some differences in the topology of this function.

The reactivity regions are distributed over the P atoms which present a lone pair, but the Fukui-basins do not have lone-pair shape, rather bonding-like shape. Another interesting change is that terminal O in this cluster presents very small reactivity. The local reactivity trend changes in the $P_4O_9$ cluster, in this case an unexpected result is present, one P atom with a lone pair, which is unreactive in terms of the Fukui description. Finally, in the cluster $P_4O_{10}$, the local reactivity could be rationalized as if the lone-pairs basin in $P_4O_6$ had migrated toward O which are placed over the lone pair regions to form the $P_4O_{10}$ cluster. In general, we can conclude that, despite the existence of structural relation between the studied clusters ($P_4O_6$-$P_4O_{10}$), the relationship between local reactivity is not obvious. Therefore, this study shows that even in these small set of P-O based clusters, the local reactivity could drastically change, which should be taken with caution in the studies that involves the reactivity of these kinds of systems.

## Conclusions

According to the coordination number of P in the phosphorus oxides ($P_4O_{6+n}$ (n=0–4)) it was possible to find different kinds of P-O bonds. These different kinds of bonds were characterized using several topological analysis. From the results it can be seen that each type of bond is independent of the oxygen atoms number in the structure. The topological results for the $P^V$-$O_c$ allowed us to infer that tetraphosphorus oxide structures with more quantity of this kind of bond could be more stable in comparison with those structures where this quantity is lower. Despite the existence of structural relation between the studied clusters ($P_4O_{6+n}$ (n= 0–4)), the relationship between local reactivity is not obvious. Therefore, this study shows that even in this small set of P-O based clusters, the local reactivity could drastically change, which should be taken with caution in the studies that involve the reactivity of these kinds of systems.

**Acknowledgment** The authors are grateful to EPM (Empresas Pública de Medellín)/CIIEN (Centro de Investigación e Innovación en Energía) and COLCIENCIAS (Departamento Administrativo de Ciencia, Tecnología e innovación) for financing the project 1115-4547-21979, and to the University of Antioquia for the financial support of the "Programa Sostenibilidad 2013-2014". WT thanks Fondecyt financial support (Grant No 11090431). NA thanks "COLCIENCIAS" and the University of Antioquia for the PhD scholarship.

## References


1. Salvadó MA, Pertierra P (2008) Theoretical study of P2O5 polymorphs at high pressure: hexacoordinated phosphorus. Inorg Chem 47(11):4884–4890
2. Engels B, Soares Valentim AR, Peyerimhoff SD (2001) About the chemistry of phosphorus suboxides. Angew Chem Int Ed 40 (2):378–381
3. Dimitrov A, Ziemer B, Hunnius W-D, Meisel M (2003) The first ozonide of a phosphorus oxide—preparation, characterization, and structure of P4O18. Angew Chem Int Ed 42(22):2484–2486
4. Klapötke TM (2003) P4O18—the first binary phosphorus oxide ozonide. Angew Chem Int Ed 42(30):3461–3462
5. Carbonnière P, Pouchan C (2008) Vibrational spectra for P4O6 and P4O10 systems: theoretical study from DFT quartic potential and mixed perturbation-variation method. Chem Phys Lett 462(4–6):169–172
6. Mielke Z, Andrews L (1989) Infrared spectra of phosphorus oxides (P4O6, P4O7, P4O8, P4O9 and P4O10) in solid argon. J Phys Chem 93(8):2971–2976
7. Jansen M, Moebs M (1984) Structural investigations on solid tetraphosphorus hexaoxide. Inorg Chem 23(26):4486–4488
8. Beattie IR, Ogden JS, Price DD (1978) The characterization of molecular vanadium oxide (V4O10), an analog of phosphorus oxide (P4O10). Inorg Chem 17(11):3296–3297
9. Sharma BD (1987) Phosphorus(V) oxides. Inorg Chem 26(3):454–455
10. Valentim ARS, Engels B, Peyerimhoff SD, Clade J, Jansen M (1998) A comparative study of the bonding character in the P4On (n=6–10) series by means of a vibrational analysis. J Phys Chem A 102(21):3690–3696
11. Mowrey RC, Williams BA, Douglass CH (1997) Vibrational analysis of P4O6 and P4O10. J Phys Chem A 101(32):5748–5752
12. Lohr LL (1990) An ab initio characterization of the gaseous diphosphorus oxides P2Ox (x=1–5). J Phys Chem 94(5):1807–1811
13. Moussaoui Y, Ouamerali O, De Maré GR (2003) Properties of the phosphorus oxide radical, PO, its cation and anion in their ground electronic states: comparison of theoretical and experimental data. Int Rev Phys Chem 22(4):641–675
14. Butler JE, Kawaguchi K, Hirota E (1983) Infrared diode laser spectroscopy of the PO radical. J Mol Spectrosc 101(1):161–166
15. Kanata H, Yamamoto S, Saito S (1988) The dipole moment of the PO radical determined by microwave spectroscopy. J Mol Spectrosc 131(1):89–95
16. Dyke JM, Morris A, Ridha A (1982) Study of the ground state of PO+using photoelectron spectroscopy. J Chem Soc, Faraday Trans 78(12):2077–2082
17. Zittel PF, Lineberger WC (1976) Laser photoelectron spectrometry of $PO^-$, $PH^-$, and $PH_2^-$. J Chem Phys 65(4):1236–1243
18. Noury S, Krokidis X, Fuster F, Silvi B (1997) TopMod Package
19. Flkiger P, Lthi HP, Portmann S, Weber J (2008) MOLEKEL 5.3. Molekel homepage. http://www.cscs.ch/molekel (accessed 20 April 2010)
20. Bader R (1990) Atoms in molecules. Oxford University Press, New York, A Quantum Theory
21. Popelier PLA (1996) MORPHY, a program for an automated "atoms in molecules" analysis. Comput Phys Commun 93:212–240
22. Geerlings P, De Proft F, Langenaeker W (2003) Conceptual density functional theory. Chem Rev 103:1793–1873
23. Chermette H (1999) Chemical reactivity indexes in density functional theory. J Comput Chem 20:129–154
24. Ayers PW, Anderson JSM, Bartolotti LJ (2005) Perturbative perspectives on the chemical reaction prediction problem. Int J Quantum Chem 101:520–534
25. Gazquez J (2008) Perspectives on density functional theory Of chemical reactivity. J Mex Chem Soc 52(1):3–10
26. Yang WT, Parr RG, Pucci R (1984) Electron density, Kohn-Sham frontier orbitals, and Fukui functions. J Chem Phys 81:2862–2863
27. Ayers PW, Levy M (2000) Perspective on "Density functional approach to the frontier-electron theory of chemical reactivity" by Parr RG, Yang W (1984). Theor Chem Acc 103:353–360
28. Perdew JP, Parr RG, Levy M, Balduz JL Jr (1982) Density-functional theory for fractional particle number: derivative discontinuities of the energy. Phys Rev Lett 49:1691–1694
29. Yang WT, Zhang YK, Ayers PW (2000) Degenerate ground states and fractional number of electrons in density and reduced density matrix functional theory. Phys Rev Lett 84:5172–5175
30. Ayers PW, Parr RG (2000) Variational principles for describing chemical reactions: the Fukui function and chemical hardness revisited. J Am Chem Soc 122:2010–2018
31. Ayers PW (2008) The continuity of the energy and other molecular properties with respect to the number of electrons. J Math Chem 43 (1):285–303
32. Parr RG, Yang W (1984) Density functional approach to the frontier-electron theory of chemical reactivity. J Am Chem Soc 106(14):4049–4050
33. Fuentealba P, Chamorro E, Cardenas C (2007) Further exploration of the Fukui function, hardness, and other reactivity indices and its relationships within the Kohn-Sham scheme. Int J Quantum Chem 107:37–45
34. Ayers PW (2006) Can one oxidize an atom by reducing the molecule that contains It? Phys Chem Chem Phys 8:3387–3390
35. Bartolotti LJ, Ayers PW (2005) An example where orbital relaxation is an important contribution to the Fukui function. J Phys Chem A 109:1146–1151
36. Melin J, Ayers PW, Ortiz JV (2007) Removing electrons can increase the electron density: a computational study of negative Fukui functions. J Phys Chem A 111:10017–10019
37. Cardenas C, Ayers PW, Cedillo A (2011) Reactivity indicators for degenerate states in the density-functional theoretic chemical reactivity theory. J Chem Phys 134(17):174103–174113
38. Flores-Moreno R (2009) Symmetry conservation in Fukui functions. J Chem Theory Comput 6(1):48–54
39. Martínez J (2009) Local reactivity descriptors from degenerate frontier molecular orbitals. Chem Phys Lett 478(4–6):310–322
40. Tiznado W, Chamorro E, Contreras R, Fuentealba P (2005) Comparison among four different ways to condense the Fukui function. J Phys Chem A 109(14):3220–3224
41. Fuentealba P, Florez E, Tiznado W (2010) Topological analysis of the Fukui function. J Chem Theory Comput 6(5):1470–1478
42. Osorio E, Ferraro MB, Oña OB, Cardenas C, Fuentealba P, Tiznado W (2011) Assembling small silicon clusters using criteria of maximum matching of the Fukui functions. J Chem Theory Comput 7(12):3995–4001
43. Florez E, Tiznado W, Mondragón F, Fuentealba P (2005) Theoretical study of the interaction of molecular oxygen with copper clusters. J Phys Chem A 109(34):7815–7821
44. Tiznado W, Ona OB, Bazterra VE, Caputo MC, Facelli JC, Ferraro MB, Fuentealba P (2005) Theoretical study of the adsorption of H on $Si_n$ clusters, (n=3–10). J Chem Phys 123(21):214302
45. Tiznado W, Oña OB, Caputo MC, Ferraro MB, Fuentealba P (2009) Theoretical study of the structure and electronic properties of Si3On−and Si6On−(n=1–6) clusters. Fragmentation and formation patterns. J Chem Theory Comput 5(9):2265–2273
46. Kohout M (2011) DGrid 4.6. Radebeul
47. Popelier PLA (2000) Atoms in molecules. An introduction. Pearson Education, Harlow